JOTCS A
Journal of the Turkish Chemical Society
Section: A
Chemistry
TURKISH CHEMICAL SOCIETY

# Examination of the Effects of Activated Carbon Produced from Coal Using Single-Step $H_3PO_4/N_2+H_2O$ Vapor Activation on the Adsorption of Bovine Serum Albumin at Different Temperatures and pH Values

**Atakan Toprak*[1] and Kadriye Bozgeyik[2]**

*[1]Department of Chemistry and Chemical Process Technology, Bülent Ecevit University, 67800 Zonguldak, Turkey[1]*

*2Department of Chemistry, Bülent Ecevit University, 67100 Zonguldak, Turkey[2]*

**Abstract:** This study examined protein adsorption equilibrium and kinetics on activated carbon (AC) that we obtained from coal by single-step $H_3PO_4$ activation under $N_2+H_2O$ vapor at 800 °C. Surface properties, pore size distribution, and volumes of AC were determined using volumetric method with $N_2$ adsorption at 77 K. Also, the textural properties were characterized by SEM-EDAX and XRD. The zeta potential values were measured to elucidate the electrostatic interactions between the protein and AC. The obtained AC discrete system was also used as an adsorbent for adsorbing bovine serum albumin (BSA) from aqueous solution. The effects of pH (4.0, 5.0, and 7.4) and temperatures (20, 30 and 40 °C) on the adsorption of BSA on AC were examined. The surface area, micropore, mesopore and total pore volumes of AC were found to be 1175 $m^2/g$, 0.477 $cm^3/g$, 0.061 $cm^3/g$ and 0.538 $cm^3/g$, respectively. The optimum temperature for AC in BSA adsorption was found to be 40 °C and the pH was found to be 4.0. The highest BSA adsorption was found to be 159 mg/g and pH to be 4.0. The experimental equilibrium data were compared with the Langmuir and Freundlich models and found to be compatible with both models. The adsorption process is best described by the pseudo-first-order kinetic model. As a result, it was found out that AC obtained by single step $H_3PO_4/N_2+H_2O$ vapor activation is an effective adsorbent for the adsorption of BSA from aqueous solution.

**Keywords:** Coal, Activated Carbon, BSA, Adsorption Isotherms, Kinetics.

**Submitted:** October 02, 2017**. Accepted:** December 22, 2017**.**

**Cite this:** Toprak A, Bozgeyik K. Examination of the Effects of Activated Carbon Produced from Coal Using Single-Step H3PO4/N2+H2O Vapor Activation on the Adsorption of Bovine Serum Albumin at Different Temperatures and pH Values. JOTCSA. 2018;5(1):219–36.

**DOI:** http://dx.doi.org/10.18596/jotcsa.341336.

***Corresponding author. E-mail:** atakantoprak2@hotmail.com. **Tel:** + 90 3725563573-156. **Fax**: + 90 3725563574.

## INTRODUCTION

Protein adsorption on surfaces is a very common phenomenon because it is the first step in many biological processes such as trans-membrane signalling or blood coagulation steps (1, 2). Protein adsorption in artificial tissue scaffolds is a key factor for a favorable vascularity (re-formation of vessels) because protein adsorption can cause thrombosis in biomedical implants interacting with blood flow (3). Moreover, protein adsorption can induce adhesion of the possible inflammation of particles, bacteria, cells and their contamination processes (4). Non-specific protein adsorption on sensor surfaces, protein chips or experiment platforms in the fields of analytical science is a serious problem that disrupts the analytical performance of devices. Indeed, there are intensive studies on biocompatible and protein-resistant materials that can be applied to biomedical implants or analytical platforms, and the vast majority of scientific publications in recent years have contributed extensively to this field (5-8). Progress in this area has taken place during the emergence of grafted polymers (such as PEG, PAA) and self-assembled monolayers (SAM) in particular. However, the rules behind protein rejection are still not fully understood, and it is still necessary to better understand the stability of selected surfaces (9-11)

Protein-surface interactions are influenced by both protein properties and surface properties. Surface energy, surface tension, polarity, surface charge, surface wetting potential and morphology are important parameters affecting protein-surface interactions (12). Scientific studies have generally chosen the type of surface adsorbent that can replace implant materials, cell walls, biosensors or membrane filters. Some typical limitations are introduced according to the experimental techniques applied to the model surfaces (such as atomic flat surfaces whose optical transparency, electrical conductivity or flexibility can be affected). Furthermore, protein is also frequently adsorbed on unmodified surfaces such as quartz, mica, glass, metal or graphite, and modified surfaces obtained with chemical modification of these surfaces (3).

Activated carbon is an adsorbent that is highly versatile in its use, with a high surface area, pore structure and a high degree of surface reactivity. Because of its unique porosity and surface morphology, it is specifically in many areas in industry such as gas adsorption, purification and separation of gaseous mixtures, removal of harmful contaminants, processing of urban and industrial wastewater, fuel cells, adsorption of large molecules and as a catalyst in drug synthesis (13-15). The activated carbons are of interest because they are easy to produce, durable and quite cheap compared to other types of adsorbents (16). The adsorption capacity of the activated carbons is due to the presence of pores suitable

to the molecular size of the adsorbent and the interest of functional groups on the surface to the adsorbent.

Two methods (physical and chemical activation) are mainly used for activated carbon production. Physical activation involves carbonization and activation with steam and $CO_2$ at high temperature. Chemical activation involves the activation of samples impregnated with various activating agents (NaOH, KOH, $H_3PO_4$, $ZnCl_2$, *etc.*) in an inert atmosphere (17, 18).

In this study, we tried to examine protein adsorption on activated carbon obtained by sonication and single-step $H_3PO_4/N_2+H_2O$ vapor activation on an coal sample taken from Zonguldak region (Zonguldak is a province located along the Black Sea coast in the northwest of Turkey, and is also known as a major center of coal production). We chose BSA as a model protein, which is a blood plasma protein. Firstly, the characterization of the activated carbon (surface area, pore distribution, micropore volume) was examined by $N_2$ adsorption at 77 K with volumetric methods, and its morphological characteristics were determined with SEM-EDAX and XRD. BSA adsorption equilibrium and kinetics on activated carbon were then examined for different temperatures and pHs. Zeta potential values were also measured to understand protein-surface interaction.

## MATERIALS AND EXPERIMENTAL

### Materials

BSA and other chemicals were purchased from Sigma Aldrich.

### Activated carbon production

Highly volatile A type bituminous coal (ASTM standards) was taken from Zonguldak region as the starting material and it was made into a size of 100-300 μm (19). Since inorganic materials such as Fe, Al, and Si in the coal sample produce water-insoluble residues such as $FePO_4$, $Al(PO_3)_3$ and $SiO_2P_2O_7$ in activation with $H_3PO_4$, they cause low pore formation and adsorption capacity in activated carbon (20, 21). For this reason, the ash removal process was carried out to eliminate the interaction of $H_3PO_4$ with the inorganic substance in the coal. In the ash removal process the coal was first mixed with 20% HCl for 3 hours at 60°C. The treated sample was washed repeatedly using hot distilled water until the pH reached about 7.0. Then the same process was repeated with 25% HF. As a result of the ash removal, the ash content was reduced to 0.4%, having initially been 4.5% (22).

For AC production, the ash-reduced coal with $H_3PO_4$ was mixed at the rate of 3:1 with magnetic stirrer (1000 rpm) at 70 °C. After the mixture was sonicated for 30 minutes at 60 °C, it was transferred to the quartz tube and kept in the drying-oven at 100 °C overnight. In this method, the water vapor connection was made after the mixture was brought to 800°C under $N_2$ (200 mL/min) in a tube furnace. The mixture was activated with $N_2$+$H_2O$ vapor for 30 min and allowed to cool under $N_2$. AC obtained after activation was washed with hot distilled water until the pH was 7.0 and then dried in an oven at 110 °C.

**AC analysis methods**: The physical characteristics of AC obtained by one-step $H_3PO_4$/$N_2$+$H_2O$ vapor activation were calculated using a Quantachrome AS 1C device with $N_2$ adsorption-desorption at 77 K in the range of 0.01-0.995 of $P/P_0$. AC was degassed under vacuum at 150°C for 5 hours before $N_2$ adsorption at 77 K. BET (Brunauer, Emmett and Teller) and Langmuir surface areas, micro ($V_{micro}$), meso ($V_{meso}$) and total pore volumes ($V_T$) were calculated using $N_2$ isotherm at 77 K. The pore size distributions were determined by DFT (Density Functional Theory) method. The micropore volume ($V_{micro}$) was calculated using the Dubinin Radushkevich (DR) model in the range of 0.01-0.05 of $P/P_0$. The total pore volume ($V_T$) was calculated from the volume value of $N_2$ isotherm at $P/P_0$.=0.995. $V_{meso}$ is obtained by subtracting $V_{micro}$ volume from $V_T$. The surface morphology and element percentage of AC were determined by using an FEI QUANTA FEG 450 (SEM-EDAX) device. The diffraction analysis of AC was measured by PAN-analytical's Empyrean device at the range of 2θ=10-90°.

**Adsorption experiments**

For the adsorption equilibrium experiment, 100 mL of BSA solutions with an initial concentration of 500 mg/L were prepared in 250 mL capped conical flasks. The pH of the BSA solutions was adjusted with pH=2.8 ($NaH_2PO_4$/$H_3PO_4$) and pH=10 ($NH_4Cl$/$NH_3$) buffers. The prepared solutions were placed in a water bath at a constant temperature and constant stirring speed (120 rpm). AC was added to these solutions at a rate of 2-12 g/L and absorbance values of the samples taken at the end of the equilibration period of 420 min were measured at a wavelength 730 nm in the UV-visible spectrophotometer. The remaining protein concentration in the solution was determined by the Lowry method. In the Lowry method, protein is first treated with alkaline copper sulfate in the presence of tartrate. This "incubation" is then followed by the addition of the Folin-phenol reagent. It is believed that the enhancement of the color reaction in the Lowry procedure occurs when the tetradentate copper complexes transfer electrons to the phospho-molybdic/phosphotungstic acid complex (Mo+6/W+6, Folin phenol reagent) (23).

To identify protein adsorption kinetics on activated carbon at pH=4, 5 and 7.4, 100 mL of BSA solution with a 500 mg/L initial concentration was taken and 6 g/L adsorbent was added onto it. Protein samples were taken from the mixture before and during the experiment at specific time intervals. Sampling continued until the solution concentration reached constant values. The protein concentration in the solutions obtained was determined by the Lowry method using the UV-visible spectrophotometer. These processes were repeated for temperatures of 20, 30 and 40°C.

**Zeta potential experiments**

The solution at the same initial concentration (500 mg/L) as in the adsorption experiments was used for the zeta potential measurements of BSA. AC suspension was prepared by 0.05 g of AC in 25 mL NaCl (0.9%) solution. Another set of BSA/AC suspension was prepared with 0.05 g of AC in 25 mL BSA (500 mg/L) solution. The pH of the suspensions was adjusted with $NaH_2PO_4.2H_2O/H_3PO_4$ (pH=2.8) and $NH_4Cl/NH_3$ (pH=10) buffers. The zeta potentials of BSA, AC and AC/BSA were determined with the use of a Brookhaven ZetaPlus instrument at constant temperature.

## RESULTS AND DISCUSSION

**AC characterization**

Figure 1 shows the DFT pore size distribution and $N_2$ adsorption-desorption isotherm of AC at 77 K obtained as a result of single-step $N_2+H_2O$ vapor activation of the mixture at 800 °C after impregnation and sonication of the coal sample of $H_3PO_4$ at the rate of 3:1. The curve of the $N_2$ adsorption isotherm of AC corresponds with Type I isotherm according to IUPAC classification (24). According to this, AC shows that it commonly has a microporous structure. It is also seen that desorption of the adsorption of $N_2$ at 77 K and $P/P_0$ do not correspond in the range of 0.4-0.99 and that hysteresis occurs, which is a result of the capillarity condensation while the gas fills in and bleeds in the mesopore. The hysteresis in AC corresponds with Type H4 according to IUPAC classification. Type H4 is known to be in activated carbon with a slit pore structure. According to the IUPAC classification, porous adsorbents are classified as micropores if they are below 20 Å and as mesopores in the range of 20-500 Å. In the DFT pore size distribution in Figure 1, it is seen that micropores and, at low rate, mesoporous structures are commonly observed. Table 1 shows the surface characteristics of AC calculated from the $N_2$ adsorption-desorption isotherm at 77 K. The BET and Langmuir surface areas of AC were found to be 1175 and 1270 $m^2/g$ respectively. In addition, micropore (calculated with DR model), mesopore and the total pore volume were found to be 0.477, 0.061 and 0.538 cc/g respectively.

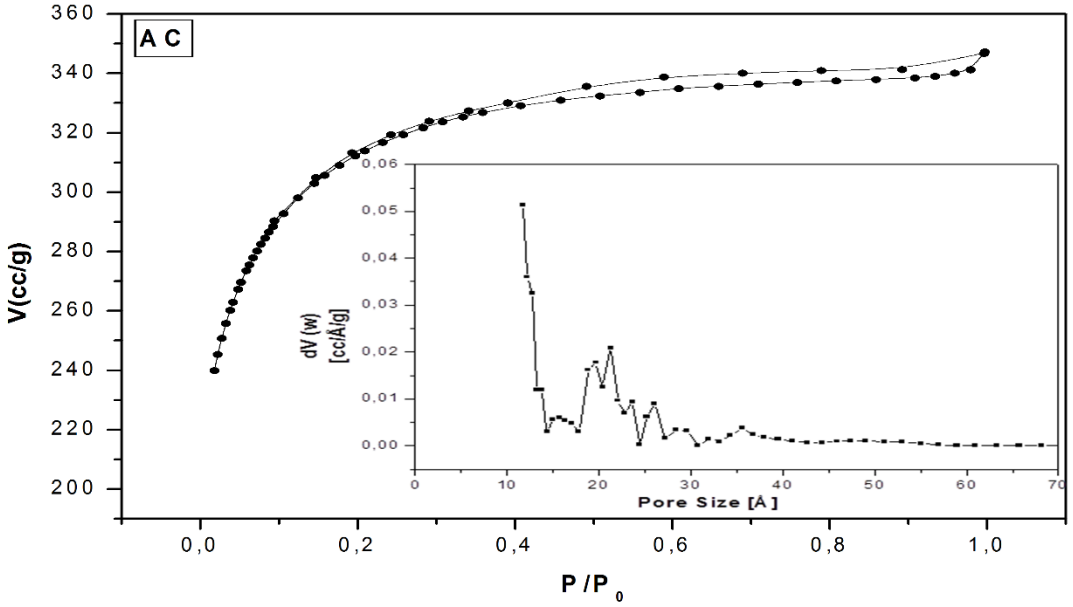


**Figure 1:** $N_2$ adsorption–desorption isotherms at 77 K and pore size distribution for AC prepared by single step $H_3PO_4/N_2+H_2O$ vapor activation at 800 °C.

**Table 1.** Surface and pore structure parameters of AC prepared by single step $H_3PO_4/N_2+H_2O$ vapor activation at 800 °C.

| Sample | Surface Area ($m^2/g$) | | Pore Volumes (cc/g) | | | Pore Sizes (Å) | |
|---|---|---|---|---|---|---|---|
| | ***BET*** | ***Lang.*** | $V_{micro}$ | $V_{meso}$ | $V_T$ | ***DFT*** | ***Average*** |
| **AC** | 1175 | 1270 | 0.477 | 0.061 | 0.538 | 11.7 | 18.3 |

The surface morphology of AC was observed with SEM-EDAX in Figure 2. When the SEM image is examined, it is seen that there are irregular macroscopic pores and cavities on the surface of AC. It can be said that these pore formations are the result of the vaporization of volatiles such as $CO_2$, CO and $H_2$ from the carbon surface during $H_3PO_4$ and that $N_2+H_2O$ vapor activation, temperature and sonication are also important parameters (25).

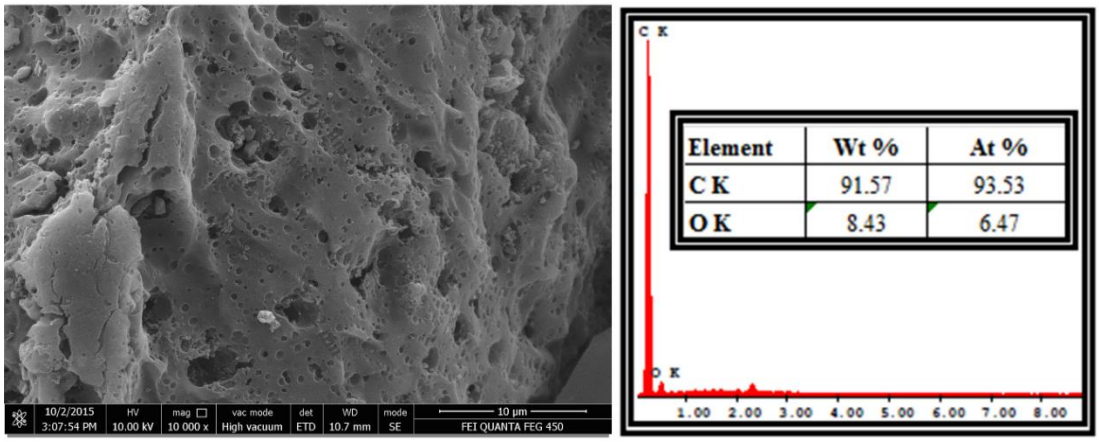


**Figure 2.** SEM image and EDAX analysis of AC.

The XRD pattern of AC is given in Figure 3. It is seen that there are three characteristic peaks in AC at approximately 25°, 43° and 79°. The peaks at 2θ=25° (002 plane) show the stacking structure of the aromatic layers and crystallinity height and 100/101 planes at 2θ=45° show the average crystallinity width. In AC, we can say that crystalline regions develop as sharp peaks at 25° in fragments. The 100/101 plane at 43° and the 110 plane at 79° in AC have weak intensity. This means that the AC shows the presence of small domains of ordered graphene sheets. Peaks at 25° and 43° have narrower and higher intensities, so we can say that it has graphene-like regular crystalline structures similar to the AC produced in the literature (26-29).

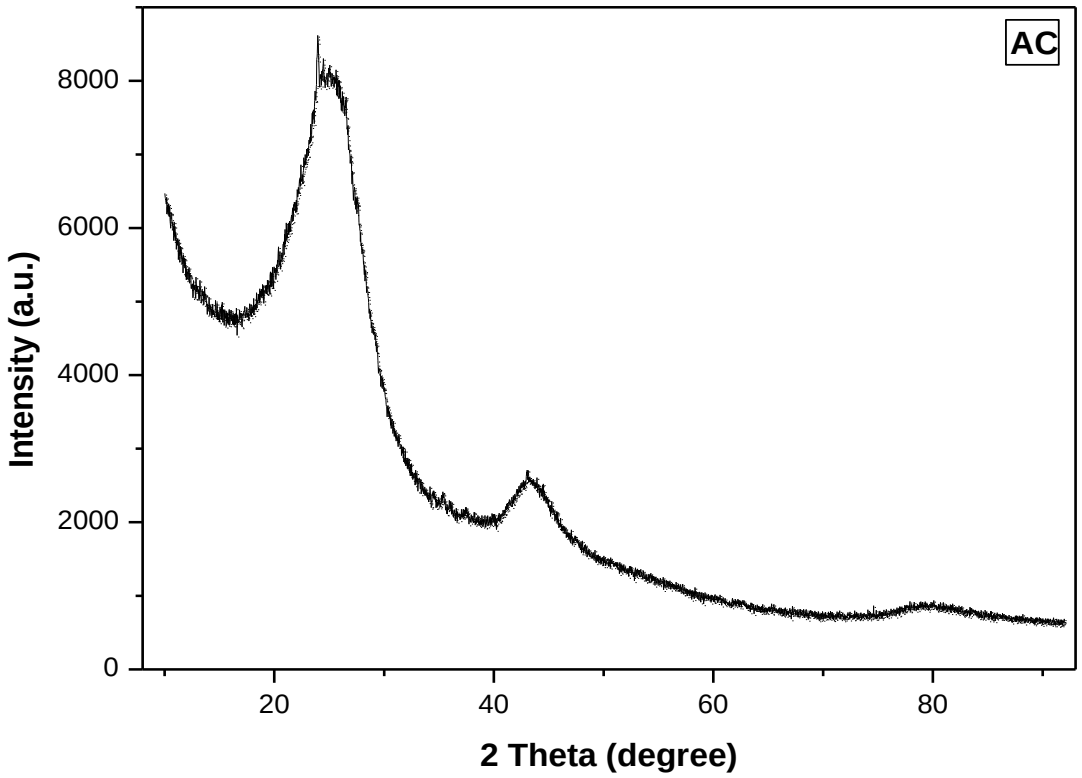


**Figure 3:** X-Ray diffraction patterns of AC.

**Effect of temperature and pH on BSA adsorption**

One of the important factors affecting protein adsorption is temperature. Proteins are subjected to a conformational change between primary structures and quaternary structures due to temperature differences. It is even the case that proteins are denaturalized due to temperature (30).

The effect of temperature on BSA adsorption on AC was determined by observing the changes in the protein concentration in the liquid phase at 20, 30 and 40 °C over time. Figures 4-6 show the effects of temperature at various pHs. In the figures for all pH environments, it is seen that the amount of BSA adsorbed onto AC generally increases as the temperature increases. The increase in adsorption capacity with increasing

temperature can be explained as a result of increases in protein activity leading diffusion to increases on the effective adsorbent surfaces (31). The optimum temperature environment for AC was found to be 40 °C at all pH values.

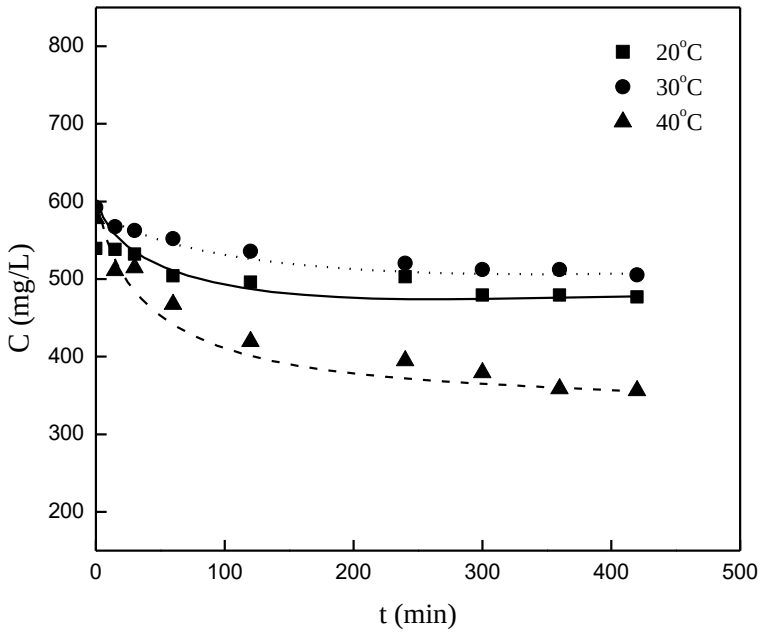


**Figure 4.** Effect of temperature on AC/BSA adsorption at pH=4.0.

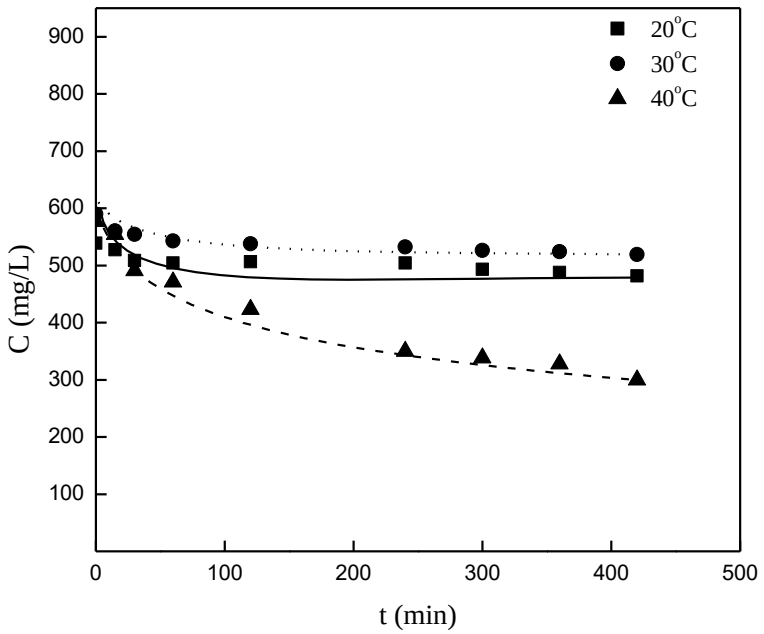


**Figure 5.** Effect of temperature on AC/BSA adsorption at pH=5.0.

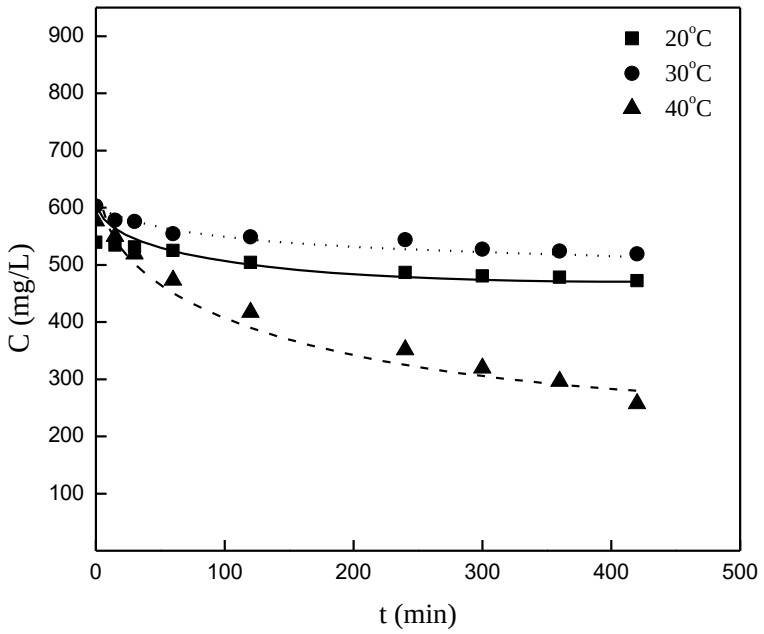


**Figure 6.** Effect of temperature on AC/BSA adsorption at pH=7.4.

**Zeta potential**

Zeta potential measurement is an easy and intelligible method to determine the presence of electrostatic interactions on the surface (32). To elucidate the electrostatic interactions between the surface and protein, the zeta potential values of the adsorbent, protein, and protein-adsorbent were measured.

The graph of zeta potential values measured for BSA, AC and AC/BSA is given in Figure 7. It is seen that zeta potential values of AC suspensions prepared with 0.15 M NaCl solution are negative ((-10)–(-30) mV) in all measured pH environments. The isoelectric point (p$I$) of BSA is found to be about 4.7. BSA has positive zeta potential values at lower pH than p$I$, and negative values at a higher pH. The interaction between positively charged BSA and negatively charged AC particles at pH 4 is a consequence of electrostatic attraction forces. For this reason, the highest protein adsorption capacity for AC was found at pH 4. Zeta potential changes also coincide with the adsorption equilibrium results obtained for AC/BSA. Zeta potential values measured for the AC/BSA also have a negative magnitude but less negative magnitude than AC. This magnitude difference occurred more at pH 5 and 7.4. This is due to the reduction of the negatively charge density on the active carbon surface after the AC surface has been coated with BSA. Although AC and BSA have negative charges at pH 5 and 7.4, it was found that protein was adsorbed on activated carbon surfaces. Even protein and substrate surface have the same charge, in vitro studies have shown that adsorption can occur for albumin. Adsorption was interpreted as an entropic

increase due to the shocks in the 'soft' α-helical structure of serum albumin despite electrostatic repulsion (33).

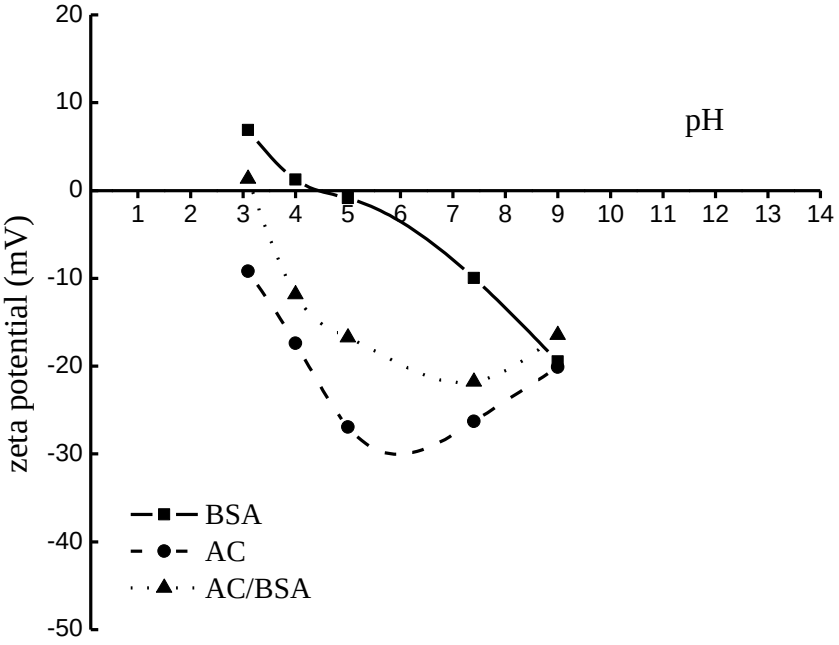


**Figure 7.** Zeta potential curve for AC/BSA adsorption.

**Adsorption equilibrium**

The BSA adsorption data are correlated with the isotherm models of Langmuir at Eq. (1) (34) and Freundlich at Eq. (2) (35),

$$\frac{1}{q_e} = \frac{1}{Q_0} + \frac{1}{Q_0 b}\frac{1}{C_e} \quad \text{(Eq. 1)}$$

$$q_e = K_f C_e^{1/n} \quad \text{(Eq. 2)}$$

where $C_e$ is the equilibrium concentration of BSA (mg/L), $Q_0$ the maximum adsorption capacity (mg/g), $b$ the Langmuir adsorption constant and $K_f$ and $1/n$ are Freundlich constants.

Experimental $q_e$ and $C_e$ values obtained for the adsorption of BSA on AC at various temperature and pH were compared with Langmuir and Freundlich models. Figures 8 and 9 show the linear graphs of Langmuir and Freundlich isotherm models given for pH 4 and 20 °C. In addition, the Langmuir and Freundlich model parameters obtained from the slope of the linear graphs for each pH and temperature, and the correlation coefficient squared ($R^2$) values indicating the compatibility of the models with the experimental data are given in Table 2. When Table 2 is examined, it is seen that experimental data at 20 °C for pH 5 and at 20 and 30 °C for pH 7.4 are not compatible with either the Langmuir or Freundlich models. The adsorption capacity calculated for the Langmuir model is $Q_0$, and it is observed

that the values increase at pH 5 and 7.4 as the temperature increases, and at pH 4, the $Q_0$ value is 160.3 mg/g at 20 °C; it decreases to 101.4 mg/g at 30 °C, and increases again to 159.0 mg/g at 40 °C. The maximum protein adsorption capacity was found to be almost the same at 20 and 40°C for pH 4. In a study conducted by Taskin *et al.* (36), the highest protein adsorption capacity for bovine serum albumin adsorption on modified activated carbon (2492 $m^2/g$) was found to be 136.77 mg/g. When the protein adsorption capacities were compared, it was found out that more BSA (160.3 mg/g) was adsorbed although the surface area of AC (1175 $m^2/g$) that we obtained was smaller than the surface area of the modified activated carbon.

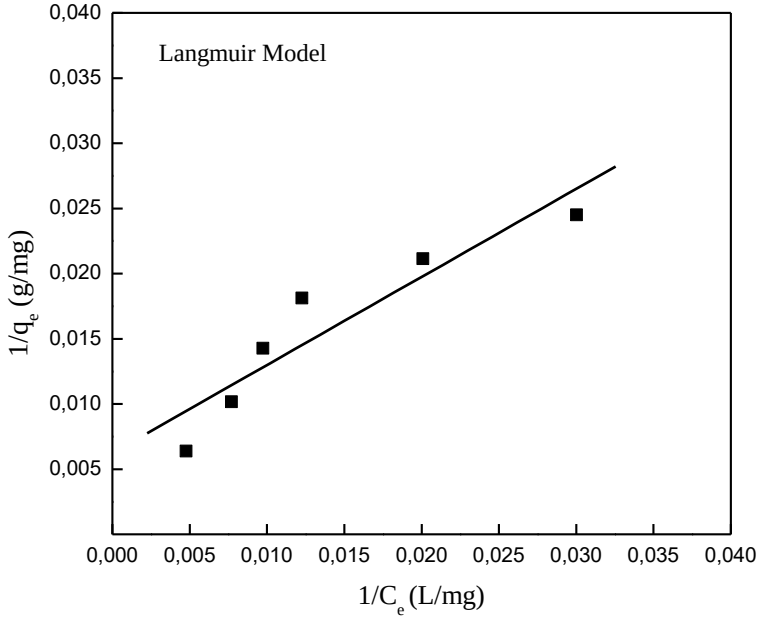


**Figure 8:** Langmuir Model curve obtained for AC/BSA adsorption at pH 4 and 20°C.

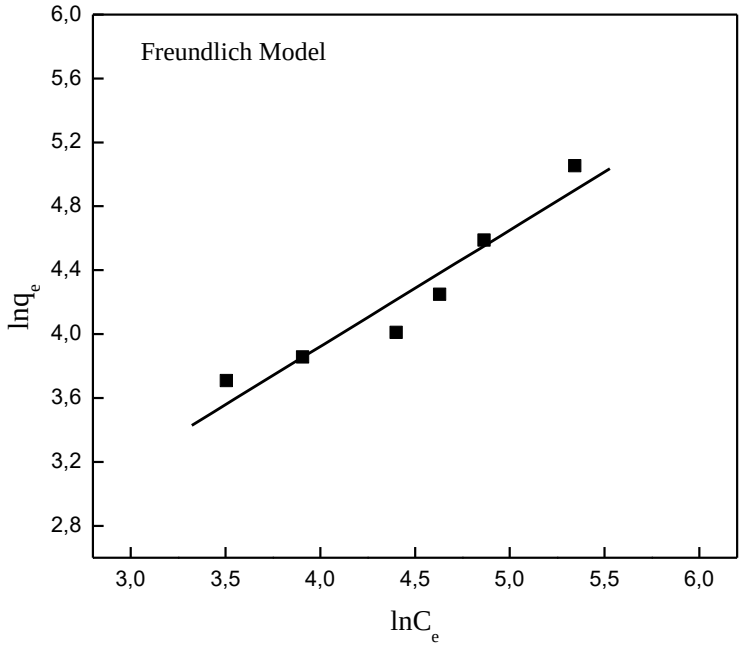


**Figure 9.** Freundlich model curve obtained for the AC/BSA adsorption at pH 4 and 20°C.

When the Freundlich model parameters are examined, it is seen that the 1/*n* values indicating the adsorption density are smaller than 1 in all pH environments. It is known that the closer the value of 1/*n* is to zero, the greater the density and heterogeneity of the adsorbed material on the adsorbent surface is (37). When the $R^2$ values in the models are close to unity, this is the indicative of the compatibility of that model with the experimental data. When the $R^2$ values of the Langmuir and Freundlich models in Table 2 are compared, it is seen that $R^2$ values are almost the same for both isotherm models.

**Table 2.** Langmuir and Freundlich model parameters calculated for AC/BSA adsorption system at different pHs and temperatures.

| ***pH*** | ***pH 4*** | | | ***pH 5*** | | | ***pH 7.4*** | | |
|---|---|---|---|---|---|---|---|---|---|
| **T (°C)** | **20** | **30** | **40** | **20** | **30** | **40** | **20** | **30** | **40** |
| ***Langmuir Model*** | | | | | | | | | |
| $Q_0$ *(mg/g)* | 160.3 | 101.4 | 159.0 | - | 40.0 | 90.2 | - | - | 71.8 |
| *b* | 0.0092 | 0.00029 | 0.0053 | - | 0.005 | 0.010 | - | - | 0.003 |
| $R^2$ | 0.86 | 0.96 | 0.77 | - | 0.90 | 0.92 | - | - | 0.91 |
| ***Freundlich Model*** | | | | | | | | | |
| $K_f$ | 2.75 | 0.052 | 2.19 | - | 2.66 | 6.02 | - | - | 1.52 |
| *1/n* | 0.728 | 0.877 | 0.692 | - | 0.386 | 0.431 | - | - | 0.548 |
| $R^2$ | 0.92 | 0.96 | 0.82 | - | 0.90 | 0.91 | - | - | 0.88 |

**Adsorption kinetics**

The kinetics of adsorption of BSA on activated carbon was studied on the basis of two simplified kinetic models, including pseudo-first-order and pseudo-second-order equations. The Lagergren pseudo-first-order kinetic model was represented as (38)

$$\log(q_e - q) = \log q_e - \frac{k_1}{2.303} t \qquad \text{(Eq. 3)}$$

and the pseudo-second-order equation was given by (39),

$$\frac{1}{(q_e - q)} = \frac{1}{q_e} + \mathrm{k}_2 t \qquad \text{(Eq. 4)}$$

where $k_1$ (1/min) and $k_2$ (g/mg min) are the rate constants of the pseudo-first-order and second-order adsorption kinetics respectively. $q_e$ is the amount of protein adsorbed on the surface of the adsorbent at equilibrium (mg/g) and $q$ is the amount of protein adsorbed at any time (mg/g).

In order to analyze the adsorption mechanism of BSA on AC, the experimental rate data obtained by keeping the initial concentration of BSA and adsorbent amounts constant at different pH values and temperature were compared with the Lagergren's pseudo-first and pseudo-second order kinetic models. In order to obtain the first- and second-order rate constants of BSA adsorption on AC, changes in log($q_e$-$q$) and 1/($q_e$-$q$) values in time at 20, 30 and 40 $^{o}$C at pH 4, 5 and 7.4 by keeping the absorbent amount constant are given in Figures 10 and 11 respectively. $k_1$, $k_2$, $q_e$ and $R^2$ values obtained by using the slope and the breakpoint of the straight lines in the graphs are given in Table 3. When the graphs and the chart obtained for AC were examined, $k_1$ values increased with increasing temperature at pH 4 and 5 but decreased with increasing temperature at pH 7.4. When $R^2$ values of the first- and second-order kinetic models were compared, $R^2$ values of the first order kinetic model were much closer to 1.0 than those of pseudo-first-order model at all temperatures and pHs. Therefore, BSA's adsorption rate on AC complies with the first-order kinetic model better. The rate of protein adsorption by the AC has been interpreted here in terms of the adherence of protein on the active sites of the adsorbent as well as its interparticle diffusion within the pores of the adsorbent (39, 40).

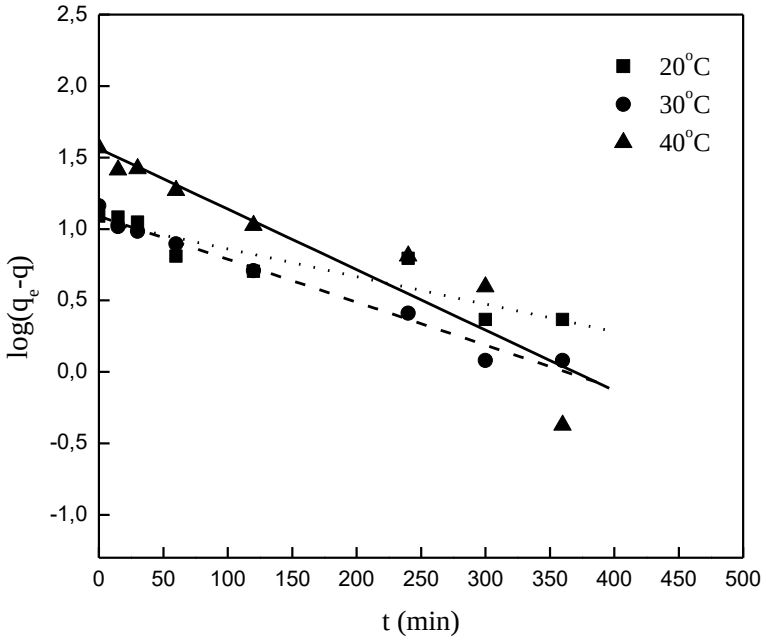


**Figure 10:** Pseudo-first-order kinetic curves for AC/BSA adsorption at pH 4.

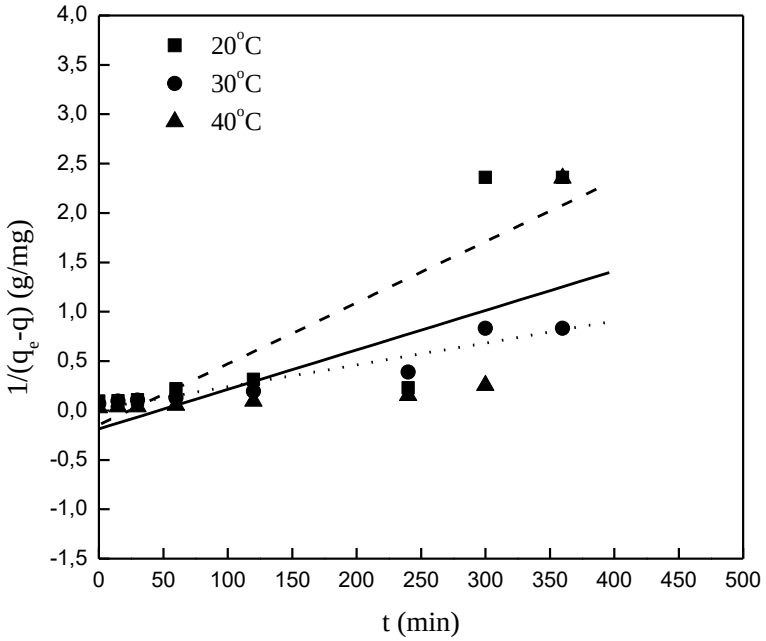


**Figure 11:** Pseudo-second-order kinetic curves for AC/BSA adsorption at pH 4.

**Table 3.** Pseoudo-first- and second-order kinetic parameters for AC/BSA adsorption system.

| ***pH*** | ***pH 4*** | | | ***pH 5*** | | | ***pH 7.4*** | | |
|---|---|---|---|---|---|---|---|---|---|
| **T (°C)** | **20** | **30** | **40** | **20** | **30** | **40** | **20** | **30** | **40** |
| **Pseudo-first-order model parameters** | | | | | | | | | |
| $k_1$ ***(1/min)*** | 0.0044 | 0.0069 | 0.0097 | 0.0046 | 0.0064 | 0.0063 | 0.0071 | 0.0068 | 0.0055 |
| $R^2$ | 0.85 | 0.98 | 0.88 | 0.81 | 0.94 | 0.99 | 0.99 | 0.92 | 0.99 |
| **Pseudo-second-order model parameters** | | | | | | | | | |
| $k_2$ ***(g/mg min)*** | 0.0062 | 0.0022 | 0.0040 | 0.0017 | 0.0029 | 0.0005 | 0.0025 | 0.0026 | 0.0003 |
| $R^2$ | 0.73 | 0.91 | 0.49 | 0.72 | 0.89 | 0.96 | 0.91 | 0.77 | 0.89 |

## CONCLUSION

AC was produced from the coal at 800 °C with single step $H_3PO_4/N_2+H_2O$ vapor activation. The surface properties and morphological characteristics of the AC produced were determined. Kinetic and electrostatic interactions and the adsorption of BSA on AC at different temperatures (20, 30 and 40 °C) and pH values (4, 5 and 7.4) were examined. According to the results obtained, the BSA adsorption capacity of AC decreased with increasing pH, but the adsorption increased with increasing temperature. However, it was also found that the BSA adsorption capacity at pH 4 decreased when the temperature increased from 20 to 30°C and had a similar adsorption capacity at 20 and 40 °C. The highest adsorption capacity was found to be 160.3 and 159 mg/g respectively at 20 and 40 °C at pH 4. Lagergren's first- and pseudo-second-order kinetic models were applied to BSA adsorption on AC at all pHs and temperatures. The results obtained show that the adsorption rate of BSA on AC complies with the first-order kinetic model in a better fashion. According to the results obtained, it can be also said that AC obtained from coal is cheaper and has potential to compete compared to other adsorbents in terms of eliminating the protein pollution.

## ACKNOWLEDGMENTS

This study was supported by Bülent Ecevit University Scientific Research Projects (project no: 2014-52349806-01). In addition, AT would like to thank Prof. Dr. Türkan Kopaç who provide them the opportunity to use her laboratory.

## REFERENCES

1. Lu JR, Zhao X, Yaseen M. Protein adsorption studied by neutron reflection. Current Opinion in Colloid & Interface Science. 2007;12(1):9-16.

2. Hinderliter A, Almeida PF, Creutz CE, Biltonen RL. Domain formation in a fluid mixed lipid bilayer modulated through binding of the C2 protein motif. Biochemistry. 2001;40(13):4181-91.

3. Rabe M, Verdes D, Seeger S. Understanding protein adsorption phenomena at solid surfaces. Advances in colloid and interface science. 2011;162(1):87-106.

4. Kalasin S, Santore MM. Non-specific adhesion on biomaterial surfaces driven by small amounts of protein adsorption. Colloids and Surfaces B: Biointerfaces. 2009;73(2):229-36.

5. Liu J, Lee ML. Permanent surface modification of polymeric capillary electrophoresis microchips for protein and peptide analysis. Electrophoresis. 2006;27(18):3533-46.

6. Roach P, Eglin D, Rohde K, Perry CC. Modern biomaterials: a review—bulk properties and implications of surface modifications. Journal of Materials Science: Materials in Medicine. 2007;18(7):1263-77.

7. Chen H, Yuan L, Song W, Wu Z, Li D. Biocompatible polymer materials: role of protein–surface interactions. Progress in Polymer Science. 2008;33(11):1059-87.

8. Cole MA, Voelcker NH, Thissen H, Griesser HJ. Stimuli-responsive interfaces and systems for the control of protein–surface and cell–surface interactions. Biomaterials. 2009;30(9):1827-50.

9. Huang N-P, Michel R, Voros J, Textor M, Hofer R, Rossi A, et al. Poly (L-lysine)-g-poly (ethylene glycol) layers on metal oxide surfaces: surface-analytical characterization and resistance to serum and fibrinogen adsorption. Langmuir. 2001;17(2):489-98.

10. Heuberger R, Sukhorukov G, Vörös J, Textor M, Möhwald H. Biofunctional polyelectrolyte multilayers and microcapsules: Control of non-specific and bio-specific protein adsorption. Advanced Functional Materials. 2005;15(3):357-66.

11. Zürcher S, Wäckerlin D, Bethuel Y, Malisova B, Textor M, Tosatti S, et al. Biomimetic surface modifications based on the cyanobacterial iron chelator anachelin. Journal of the American Chemical Society. 2006;128(4):1064-5.

12. Hlady V, Buijs J, Jennissen HP. [26] Methods for studying protein adsorption. Methods in enzymology. 1999;309:402-29.

13. Liou T-H. Development of mesoporous structure and high adsorption capacity of biomass-based activated carbon by phosphoric acid and zinc chloride activation. Chemical Engineering Journal. 2010;158(2):129-42.

14. Tsai W, Chang C, Wang S, Chang C, Chien S, Sun H. Preparation of activated carbons from corn cob catalyzed by potassium salts and subsequent gasification with $CO_2$. Bioresource Technology. 2001;78(2):203-8.

15. Hsu L-Y, Teng H. Influence of different chemical reagents on the preparation of activated carbons from bituminous coal. Fuel Processing Technology. 2000;64(1):155-66.

16. Lussier MG, Shull JC, Miller DJ. Activated carbon from cherry stones. Carbon. 1994;32(8):1493-8.

17. Hayashi J, Muroyama K, Gomes VG, Watkinson AP. Fractal dimensions of activated carbons prepared from lignin by chemical activation. Carbon. 2002;40(4):630-2.

18. Khalili NR, Campbell M, Sandi G, Golaś J. Production of micro-and mesoporous activated carbon from paper mill sludge: I. Effect of zinc chloride activation. Carbon. 2000;38(14):1905-15.

19. Kabe T, Ishihara A, Qian EW, Sutrisna IP, Kabe Y. Coal and coal-related compounds: structures, reactivity and catalytic reactions: Elsevier; 2004.

20. Teng H, Yeh T-S, Hsu L-Y. Preparation of activated carbon from bituminous coal with phosphoric acid activation. Carbon. 1998;36(9):1387-95.

21. Jagtoyen M, Thwaites M, Stencel J, McEnaney B, Derbyshire F. Adsorbent carbon synthesis from coals by phosphoric acid activation. Carbon. 1992;30(7):1089-96.

22. Kopac T, Toprak A. Preparation of activated carbons from Zonguldak region coals by physical and chemical activations for hydrogen sorption. International Journal of Hydrogen Energy. 2007;32(18):5005-14.

23. Lowry OH, Rosebrough NJ, Farr AL, Randall RJ. Protein measurement with the Folin phenol reagent. Journal of biological chemistry. 1951;193(1):265-75.

24. Gregg SJ, Sing KSW. Adsorption, surface area, and porosity: Academic Press; 1991.

25. Fu K, Yue Q, Gao B, Sun Y, Zhu L. Preparation, characterization and application of lignin-based activated carbon from black liquor lignin by steam activation. Chemical Engineering Journal. 2013;228:1074-82.

26. Lua AC, Yang T. Effect of activation temperature on the textural and chemical properties of potassium hydroxide activated carbon prepared from pistachio-nut shell. Journal of colloid and interface science. 2004;274(2):594-601.

27. Jung M-W, Ahn K-H, Lee Y, Kim K-P, Rhee J-S, Park JT, et al. Adsorption characteristics of phenol and chlorophenols on granular activated carbons (GAC). Microchemical Journal. 2001;70(2):123-31.

28. Ji Y, Li T, Zhu L, Wang X, Lin Q. Preparation of activated carbons by microwave heating KOH activation. Applied surface science. 2007;254(2):506-12.

29. Qu D. Studies of the activated carbons used in double-layer supercapacitors. Journal of Power Sources. 2002;109(2):403-11.

30. Vidal CV, Juan AO, Muñoz AI. Adsorption of bovine serum albumin on CoCrMo surface: effect of temperature and protein concentration. Colloids and Surfaces B: Biointerfaces. 2010;80(1):1-11.

31. Lu C, Chung Y-L, Chang K-F. Adsorption thermodynamic and kinetic studies of trihalomethanes on multiwalled carbon nanotubes. Journal of hazardous materials. 2006;138(2):304-10.

32. Lee W-K, Ko J-S, Kim H-M. Effect of electrostatic interaction on the adsorption of globular proteins on octacalcium phosphate crystal film. Journal of colloid and interface science. 2002;246(1):70-7.

33. Znidarsic WJ, Chen I-W, Shastri VP. ζ-potential characterization of collagen and bovine serum albumin modified silica nanoparticles: a comparative study. Journal of materials science. 2009;44(5):1374-80.

34. Langmuir I, The constitution and fundamental properties of solids and liquids: Part I. solids. Journal of the american chemical society. 1916;38: 2221-2295.

35. Freundlich H, Colloid and capillary chemistry. Methuen, London. 1926, pp 110-114.

36. Taşkın M, Özbek S, Demirhan E, Özbek B. BSA adsorption onto commercial activated carbon modified by microwave assisted chemical activation. 2016.

37. Uğurlu M. Adsorption of a textile dye onto activated sepiolite. Microporous and mesoporous Materials. 2009;119(1):276-83.

38. Largergren S. Zur theorie der sogenannten adsorption geloster stoffe. Kungliga Svenska Vetenskapsakademiens. Handlingar. 1898;24(4):1-39.

39. Ho Y-S, McKay G. Pseudo-second order model for sorption processes. Process biochemistry. 1999;34(5):451-65.

40. Orumwense F-F-O, Removal of lead from water by adsorption on a kaolinitic clay. J. Chem. Technol. Biotechnol. 1996;65:363.